

# Autonomous collision detection and avoidance for ARAGON USV: Development and field tests

Jungwook Han<sup>1</sup> | Yonghoon Cho<sup>2</sup> | Jonghwi Kim<sup>2</sup> | Jinwhan Kim<sup>2</sup>  |  
 Nam-sun Son<sup>1</sup> | Sun Young Kim<sup>1</sup>

<sup>1</sup>Maritime Safety and Environmental Research Division, KRISO, Daejeon, Republic of Korea

<sup>2</sup>Department of Mechanical Engineering, KAIST, Daejeon, Republic of Korea

## Correspondence

Jinwhan Kim, Department of Mechanical Engineering, KAIST, Daejeon 34141, Republic of Korea.  
 Email: jinwhan@kaist.ac.kr

## Funding information

The Ministry of Oceans and Fisheries, Korea, Grant/Award Number: PMS3870; Korea Research Institute of Ships and Ocean Engineering, Grant/Award Number: PES3050

## Abstract

This study addresses the development of algorithms for multiple target detection and tracking in the framework of sensor fusion and its application to autonomous navigation and collision avoidance systems for the unmanned surface vehicle (USV) Aragon. To provide autonomous navigation capabilities, various perception sensors such as radar, lidar, and cameras have been mounted on the USV platform and automatic ship detection algorithms are applied to the sensor measurements. The relative position information between the USV and nearby objects is obtained to estimate the motion of the target objects in a sensor-level tracking filter. The estimated motion information from the individual tracking filters is then combined in a central-level fusion tracker to achieve persistent and reliable target tracking performance. For automatic ship collision avoidance, the combined track data are used as obstacle information, and appropriate collision avoidance maneuvers are designed and executed in accordance with the international regulations for preventing collisions at sea (COLREGs). In this paper, the development processes of the vehicle platform and the autonomous navigation algorithms are described, and the results of field experiments are presented and discussed.

## KEY WORDS

autonomous navigation, multiple target tracking, sensor fusion, unmanned surface vehicle

## 1 | INTRODUCTION

With the improvement of computer performance and sensing technologies, unmanned surface vehicles (USVs), also known as unmanned surface vessels, have attracted significant attention for their potential applications to performing time-consuming and/or dangerous missions such as patrol, surveillance and reconnaissance, environmental monitoring, and inspection of marine structures. In line with this study trend, a number of research institutes and companies have been conducting related research projects to develop USV hardware platforms and associated software algorithms.

For safe USV operation, autonomous navigation technologies, including path planning, guidance and control, obstacle detection, and mapping, are required. In particular, automatic detection of surrounding objects and their motion estimation are key aspects, and reliable and robust performance in a wide variety of environmental conditions are necessitated. In maritime traffic environments, the information of surrounding vessels can be obtained from navigational aid systems such as the automatic identification system (AIS), very-high-frequency radiotelephony, and the electronic chart display and information system. Among these, AIS significantly contributes to maritime traffic safety by providing maritime mobile service identity,

This is an open access article under the terms of the Creative Commons Attribution-NonCommercial-NoDerivs License, which permits use and distribution in any medium, provided the original work is properly cited, the use is non-commercial and no modifications or adaptations are made.

© 2020 The Authors. *Journal of Field Robotics* published by Wiley Periodicals, Inc.

position, course, and speed information of surrounding vessels with no need for much processing procedures. However, the AIS information is not always available because not all ships are equipped with the device (only regulated under certain ship conditions such as voyaging ships above 300 gross tonnage or passenger ships). Furthermore, GPS signals are vulnerable to natural interference or intentional attacks, which can induce deterioration of signal reception by a GPS receiver integrated with AIS. Therefore, an additional sensing approach is required to detect surrounding ships whose motion information cannot be obtained from AIS equipment.

Marine radars are one of the most common navigation sensors used by marine vessels. Radars can provide relative bearing and range of surrounding vessels over a wide area with a reasonable detection performance. However, the radar detection performance degrades when the sensor suffers from a blind zone at close range due to its sensing characteristics and environmental disturbances. Additionally, radars have a slow sampling rate and low resolution; thus their detection performance drops off when recognizing a high-speed vessel or a small object protruding above the water surface. Therefore, additional sensors are necessary to enhance the autonomous situational awareness capabilities of USV systems.

In fact, optical sensors such as lidars and cameras have been successfully used for many robotics applications, and they can be used to detect close range obstacles in a radar's blind zone at a relatively high sampling rate. Three-dimensional (3D) lidars consist of multiple laser beams arranged vertically to collect surrounding obstacle information by rotating the lasers to achieve a full 360° environmental view. The sensors can be used to obtain precise relative bearing and range of close-range obstacles in the radar's blind zone. However, the effective sensing range is limited due to the relatively low angular resolution in the vertical direction, which brings few returns from a small-sized obstacle. On the other hand, cameras have relatively high angular resolution, and thus they can enhance the detectability of short- or mid-range targets. The integration of these two sensors can lead to an ideal combination to improve the performance of target detection compared to that of the conventional radar-only-based approach.

In this study, we introduce multiple target tracking based on sensor fusion and collision avoidance for autonomous maritime operation and its application to a new 8 m long USV system named "Aragon" developed by the Korea Research Institute of Ships and Ocean Engineering (KRISO). The Aragon USV system incorporates a suite of detection sensors consisting of radar, lidar, electro-optical (EO) camera, and infrared (IR) camera systems. In the authors' previous work, target tracking was introduced and implemented using an EO camera based on a classical feature-based detection approach (Park, Cho, Yoo, & Kim, 2015; Park, Kim, & Son, 2015) and using sensor fusion of radar and lidar measurements (Han & Kim, 2017), respectively. In this study, all the measurements by the onboard sensors (i.e., radar, lidar, and EO/IR cameras) are combined and fused for more reliable object detection and persistent target tracking. The combined track data are used as obstacle information

by the collision avoidance system and appropriate collision avoidance maneuvers are designed and executed in accordance with the international regulations for preventing collisions at sea (COLREGS) adopted by the International Maritime Organization (IMO; Commandant, 1999). To verify the performance of the developed target tracking and autonomous collision avoidance algorithms, field experiments were conducted in a wide range of environmental conditions using the developed USV system, and the results of the field tests are presented and discussed.

## 2 | RELATED WORK

Over the last several decades, various types of USV systems have been developed for a variety of missions and applications (Elkins, Sellers, & Monach, 2010; Huntsberger, Aghazarian, Howard, & Trotz, 2011; Sonnenburg et al., 2010; Sonnenburg & Woolsey, 2013; Wolf et al., 2010). Initially, USV systems were mainly developed for military purposes such as mine countermeasures, antisubmarine warfare, and maritime security (Bertram, 2008; Elkins et al., 2010; Huntsberger et al., 2011). Research and educational institutes have also worked to develop low-cost and small-size USV platforms with commercially available off-the-shelf components (Curcio, Leonard, & Patrikalakis, 2005; Han, Park, Kim, & Kim, 2015; Sonnenburg et al., 2010; Sonnenburg & Woolsey, 2013).

To provide vehicle autonomy for USV platforms, a great amount of research has been conducted on various techniques for autonomous navigation, obstacle detection, and collision avoidance. In particular, marine radars are commonly used as a sensor for ship detection and tracking. Various types of marine radars, such as S-band and X-band radars, have been applied to marine vessels and X-band radars have been mainly used for collision detection and avoidance. With X-band radars, the motion and physical size of targets were estimated in a joint probabilistic data association tracker (Vivone, Braca, & Errasti-Alcalá, 2015), a Bayesian network-based method was applied on multiple frame-by-frame radar images for an effective target tracking (Ma, Chen, Yan, Chu, & Wang, 2016), and multiple motion models were incorporated into an alpha-beta-tracking filter (Kazmierski, 2011).

With the advancement of optical sensor technology, some studies have suggested the use of cameras and lidar sensors for target motion analysis of close-range obstacles in marine environments (Prasad, Rajan, Rachmawati, Rajabally, & Quek, 2017). A monocular camera provides bearing information, and relative range information can be indirectly estimated from the bearing changes in the framework of bearing-only tracking. Feature-based image processing techniques were applied to detect targets on camera images and their motions were estimated by tracking filters (Farina, 1999; Frew & Rock, 2003; Park, Kim, et al., 2015). For ship detection, dynamic background subtraction and optical flow methods were applied (Bloisi & Iocchi, 2009; Hu, Yang, & Huang, 2011; Y. Zhang, Li, & Zang, 2017), and edge-based segmentation and histogram of oriented gradient were proposed to be used (Eum, Bae, Yoon, & Kim, 2015).

Furthermore, deep-learning techniques, such as faster regions with convolutional neural network (R-CNN) features (Ren, He, Girshick, & Sun, 2017), single-shot multibox detector (SSD; Liu et al., 2016), and you only look once (YOLO; Redmon & Farhadi, 2017), have been applied to enhance the vision-based detection performance (Y. Zhang, Li, et al., 2017). Recently, 3D lidars, which are regarded to be essential sensors for autonomous cars, have also been applied to marine vehicles for detecting dynamic and static obstacles in close range (Elkins et al., 2010; Han & Kim, 2017, 2019; Papadopoulos, Kurniawati, Shariff, Wong, & Patrikalakis, 2014).

To acquire more accurate target state estimates in a broader coverage, multi-sensor tracking approaches were introduced (Elkins et al., 2010; Liggins, Hall, & Llinas, 2017), and multi-radar tracking for maritime surveillance was performed by designing a tracking filter (Nikolić et al., 2016). Radar and lidar measurements were combined into a tracking filter for persistent target tracking (Han & Kim, 2017), and camera and lidar measurements were combined into a radar-based detection algorithm to enhance the detection performance by minimizing the radar's blind zone (Elfes, 1989; X. Zhang, Wang, & Cheng, 2017). Additionally, a suite of sensors including radar, camera, lidar, and AIS was employed and their measurements were combined to perceive surrounding environments (Elkins et al., 2010).

Studies addressing automatic collision avoidance have been conducted and verified with field experiments for the autonomous operation of marine vehicles in maritime traffic situations (Blaich, Rosenfelder, Schuster, Bittel, & Reuter, 2012; Perera, Ferrari, Santos, Hinostroza, & Soares, 2015; Tang et al., 2015). With USV systems developed on commercial kayak platforms, a study of automatic collision avoidance by using a monocular camera was conducted (Park, Cho, et al., 2015) and a protocol-based collision avoidance method was implemented in a behavior-based control

framework (Benjamin, Leonard, Curcio, & Newman, 2006). Also, a collision-avoidance experiment was performed using a model predictive control (Hagen, Kufoalor, Brekke, & Johansen, 2018) and a velocity obstacle-based collision avoidance algorithm was tested on a maritime combat vessel (Kuwata, Wolf, Zarzhitsky, & Huntsberger, 2014).

### 3 | SYSTEM OVERVIEW

The Aragon USV system developed by KRISO is shown in Figure 1. The platform is based on a monohull planing boat with a length of 8.0 m. The integrated USV system includes a waterjet propulsion system, various navigation and perception sensors, communication systems, and processing units. The hardware and software system components are described in Table 1.

#### 3.1 | Hardware system

Figure 2 shows the hardware system architecture including navigation and perception sensors, propulsion system, and processing units to implement autonomous navigation algorithms. A real-time kinematic global positioning system (RTK-GPS) and an inertial navigation system (INS) are installed on the USV platform and their measurements are combined to obtain accurate and reliable vehicle motion information.

The navigation sensor data from RTK-GPS and INS are collected by a serial device server, which converts serial data to transmission control protocol/internet protocol (TCP/IP) packets for data transmission to multiple onboard processing units (i.e., embedded computers). The processing units implement navigation



**FIGURE 1** Aragon unmanned surface vehicle [Color figure can be viewed at [wileyonlinelibrary.com](http://wileyonlinelibrary.com)]

**TABLE 1** Summary of the Aragon unmanned surface vehicle system

(a) Platform specifications	
Item	Description
Dimension	8.0 m (length) × 2.4 m (breadth)
Draft	0.42 m
Weight	3,000 kg (in air)
Propulsion	Diesel engine with single waterjet
Maximum speed	>44 knots
Power	570 hp
Operating hours	<15 hr (per refuel)

(b) Onboard detection sensors	
Item	Description <sup>a</sup>
Pulse radar	9,410 ± 30 MHz operating frequency (X-band), 0.25–120 NM range scale, 1. 9°(horiz.)/20°(vert.) beam width
FMCW radar	9.3–9.4 GHz operating frequency (X-band), 0–36 NM range scale, 5. 2°(horiz.)/25°(vert.) beam width
EO	62.8° × 36.8° FOV, 1,944 × 1,104 resolution
IR	3.7–4.8 μm bandwidth, 28° × 22° FOV
Lidar	0.05–100 m range, ±20 mm range accuracy, 1.33° vertical angular resolution, 360. 0°(horiz.)/41. 3°(vert.) FOV

<sup>a</sup>The performance specifications are provided by the manufacturers. The actual performance may differ depending on operating conditions.

data integration, multiple object detection/tracking, and autonomous collision avoidance. The computers are networked by an Ethernet hub to share their outputs via a user datagram protocol packet.

To perceive and recognize external environmental conditions, exteroceptive sensors including radars, lidar, and cameras are installed with an AIS transceiver. From the top of the sensor stack, the 3D lidar, frequency-modulated continuous-wave (FMCW) radar, EO/IR camera module with a pan-tilt-zoom system, and

pulse radar are mounted in a configuration that accommodates the sensor characteristics and minimizes the interference between them. Raw sensor data from the lidar (Velodyne HDL-32E, Velodyne), the FMCW radar (Simrad 4G radar, Simrad), and the cameras can be accessed by an Ethernet communication interface; thus the data are directly transmitted to their processing units for automatic target detection. A radar scan converter is used to generate a radar image by digitizing the analog signals from the pulse radar (Furuno FAR-2117, Furuno).

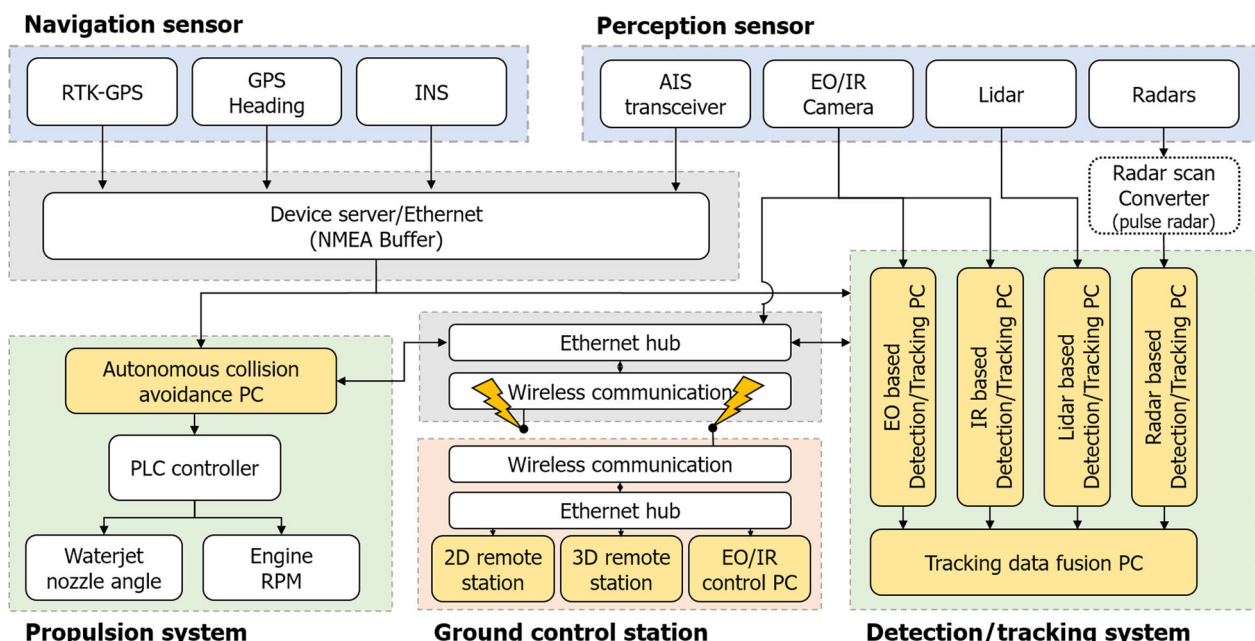


**FIGURE 2** Hardware system architecture of the unmanned surface vehicle. 3D, three dimensional; AIS, automatic identification system; EO, electro-optical; INS, inertial navigation system; IR, infrared; RTK-GPS, real-time kinematic global positioning system [Color figure can be viewed at [wileyonlinelibrary.com](http://wileyonlinelibrary.com)]

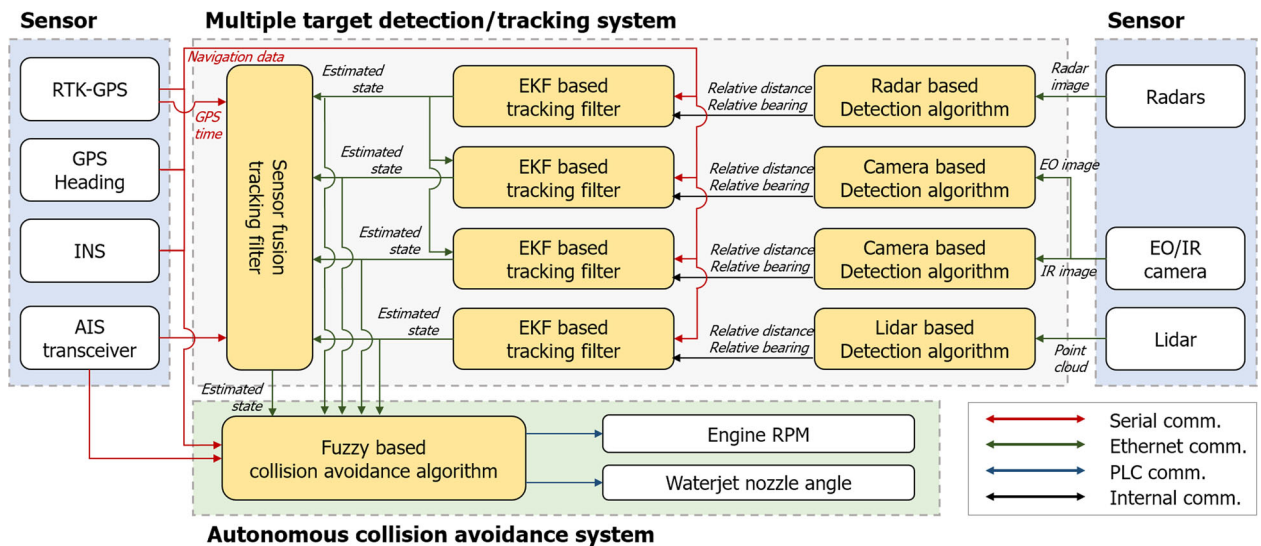


**FIGURE 3** Software system architecture of the unmanned surface vehicle. AIS, automatic identification system; EKF, extended Kalman filter; EO, electro-optical; INS, inertial navigation system; IR, infrared; RTK-GPS, real-time kinematic global positioning system [Color figure can be viewed at [wileyonlinelibrary.com](http://wileyonlinelibrary.com)]

### 3.2 | Software system

Figure 3 depicts the software system architecture consisting of the automatic target detection/tracking algorithm and the autonomous collision avoidance algorithm. The onboard exteroceptive sensors provide their measurements in the sensor-referenced frame; thus the navigation data are used to transform the sensor measurements to the global frame of reference and locate the target position (i.e., latitude/longitude).

Given the sensor measurements, the relative bearing and range information is extracted from automatic target detection algorithms and used to estimate the motion of targets in individual tracking filters. The tracking results are then combined in a central-level fusion tracker. The autonomous collision avoidance system receives the estimated motion data from both the sensor-level tracking filters and the fusion tracker and selects the tracking data to be used as obstacle information for automatic collision avoidance. An efficient collision-free route is computed from the collision avoidance algorithm, and autopilot is applied to follow the computed route.

## 4 | ALGORITHMS

### 4.1 | Sensing and object detection

For target motion analysis, the relative bearing and range information between the USV and target ships is required, and the tracking performance heavily depends on the accuracy and reliability of the relative position information. Therefore, an appropriate detection algorithm is required to extract maritime target objects from sensor measurements by minimizing noise due to glints of sunlight, wave, and ship-induced wake on the water surface.

#### 4.1.1 | Radar

A sequence of preprocessing of radar images is conducted before applying the object detection and tracking algorithms (Han & Kim, 2017), since both real target objects and unwanted echoes (i.e., clutter) are included in a radar image. The sensitivity time control and fast time constant algorithms are applied to suppress sea and rain clutter, and the areas reflected from landmass are excluded by designating a region of interest appropriately on the radar image.

The simplest way of target extraction is to threshold feature points in the preprocessed radar image with a fixed threshold value. However, the signal strength of a target is dependent not only on the target's size but also on various factors such as surface reflectivity and operating conditions. In this study, a dynamic thresholding method is applied on the radar image using the cell averaging constant false alarm rate (CA-CFAR) detector (Cambridge Pixel Ltd., 2018; Rohling, 1983). In the algorithm, a window mask whose size varies with the size of targets of interest is defined and then used to extract the signals that are sufficiently stronger than the signals from the local background. The extracted signals are classified as a single target, and the weighted center of each target is used for target tracking. The detection sequence and examples of the resulting images are shown in Figure 4.

#### 4.1.2 | Lidar

Lidars provide accurate relative bearing and range information of targets in the surrounding environment. In this study, the Velodyne HDL-32E scanner is used to obtain point cloud data reflected from surrounding environments. The collected data are expressed in the body-fixed frame which is stabilized by compensating for the roll and pitch angles of the vehicle.

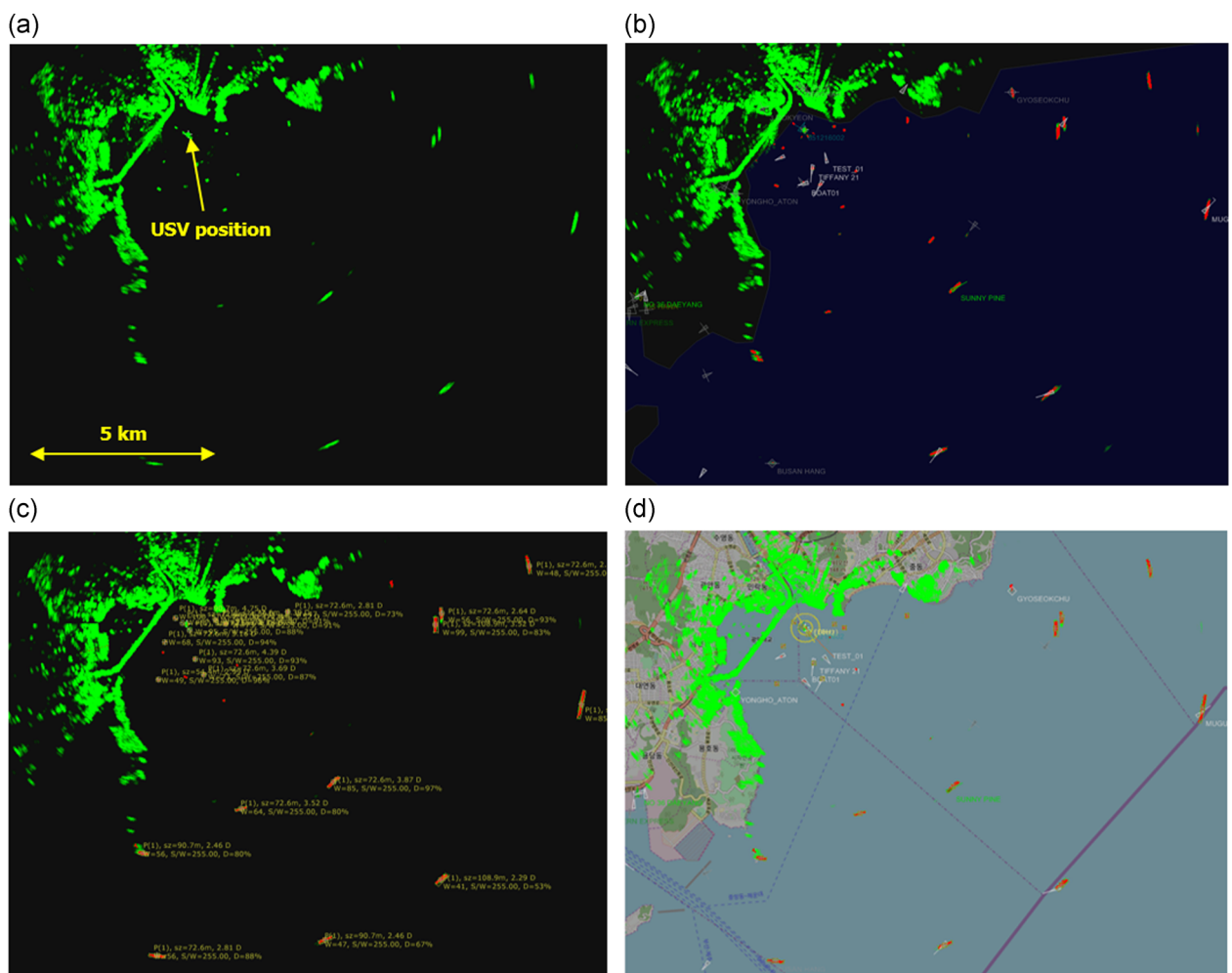


**FIGURE 4** Target detection sequence of a radar image. (a) Raw radar image. Radar signals are represented with green blobs. (b) Preprocessed radar image after applying the sensitivity time control and fast time constant filtering algorithms on a designated region of interest area. (c) Target detection results on the preprocessed radar image. (d) Final detection results. Target objects obtained from the detection algorithm are overlaid on the nautical chart. USV, unmanned surface vehicle [Color figure can be viewed at [wileyonlinelibrary.com](http://wileyonlinelibrary.com)]

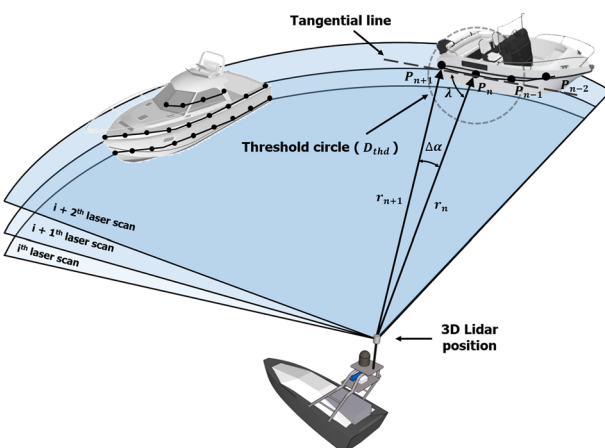


**FIGURE 5** Point cloud segmentation on multiple two-dimensional (2D) scanning planes of the 3D lidar to detect surrounding traffic ships. Point cloud data reflected from the surfaces of ships are described in black dots and they are assigned to an identical object by the point-distance-based-segmentation algorithm [Color figure can be viewed at [wileyonlinelibrary.com](http://wileyonlinelibrary.com)]

To extract feature points reflected from target objects, a clustering algorithm is required. In the authors' previous work, the Gaussian-means (G-means) algorithm was applied to find the number of obstacles and position coordinates of their centers in known environments using a 2D lidar (Han et al., 2015). The clustering algorithm has relatively high computational complexity (Hamerly & Elkan, 2003), so the approach is limited to handle a large amount of point cloud data provided by a 3D lidar. Therefore, in this study, a point-distance-based-segmentation (PDBS) algorithm is applied to ensure the online data processing (Premeida & Nunes, 2005). The PDBS algorithm extracts a boundary point from which a new cluster begins or ends by comparing the Euclidean distance between neighboring points with a threshold value obtained from the adaptive breakpoint detector (Borges & Aldon, 2004). The threshold value  $D_{\text{thd}}$  is defined on consecutive scanned points  $p_n$  and  $p_{n+1}$ , which can be written as

$$D_{\text{thd}} = r_n \times \frac{\sin(\Delta\alpha)}{\sin(\lambda - \Delta\alpha)} + 3\sigma_r, \quad (1)$$

where  $r_n$  represents the range measurement of the  $n$ th point,  $\Delta\alpha$  represents angle difference between the two points, and  $\lambda$  represents

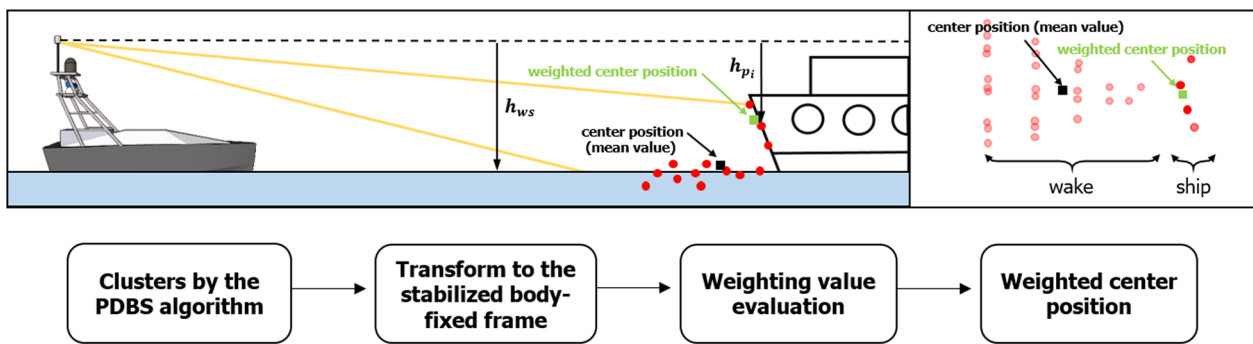


**FIGURE 6** Illustration of the weighted center position estimation. The three-dimensional lidar collects point cloud data reflected from both the surface of a ship hull and the ship-induced wake on the water surface. The weighted center position of the ship is obtained considering the height distributions of the reflected point cloud data [Color figure can be viewed at [wileyonlinelibrary.com](http://wileyonlinelibrary.com)]

the acceptable angle between the incident ray and the pseudo tangential line of the point on the surface. The residual variance of range measurement,  $\sigma_r$ , is associated with the measurement noise. If the distance between the two points  $p_n$  and  $p_{n+1}$  is below the threshold value, these two points are assigned to an identical cluster. The employed scheme is described in Figure 5.

Given the assigned point cloud data of a cluster, a weighted center position of the cluster is estimated to minimize the error induced by false measurements. In marine environments, the noise components are primarily result from the reflections caused by ship-induced wake on the water surface. To reduce the noise, the weighted center is estimated by employing a weighting value which is obtained by normalizing the vertical distance between the height of water surface  $h_{ws}$  and the  $i$ th point  $s p_i = [x_i \ y_i \ z_i]^T$  in the stabilized body-fixed frame. The associated equation to determine the weigh value is written as

$$h_{pi} = \max(z_i - h_{ws}, 0). \\ w_i = \frac{h_{pi}}{\sum_{i=1}^n h_{pi}}. \quad (2)$$

The weighted center position  $C$  of a cluster is obtained by  $C = PW$ , where  $P = [s p_1 \ s p_2 \ \dots \ s p_n]^T$  represents point cloud data and  $W = [w_1 \ w_2 \ \dots \ w_n]^T$  represents the weighting vector. The illustration of the employed weighting approach is depicted in Figures 6 and 7.

#### 4.1.3 | Cameras

For vision-based target detection, we initially applied a classical feature-based detection algorithm on a camera image (Park, Cho, et al., 2015; Park, Kim, et al., 2015). The algorithm provides reasonable performance in well-configured and steady illumination conditions. However, the parameter tuning of the feature-based detection algorithm is rather challenging and sensitive to real-world varying environmental conditions. For robust and reliable target ship detection without intensive parameter tuning during operations, a deep-learning-based detection algorithm, which has recently been successfully adopted in related applications, is employed in this study.

As deep-learning technologies have been actively developed to solve challenging computer vision problems, various object detection algorithms such as YOLO (Redmon & Farhadi, 2017), faster R-CNN (Ren et al., 2017), and SSD (Liu et al., 2016) have been introduced. In this study, the SSD algorithm was selected and used considering both its computational efficiency and detection accuracy after some preliminary performance comparison of the above-mentioned object detection methods in our applications.

The SSD is a feed-forward convolutional network that produces bounding boxes determining the location of objects and the scores representing classes of the objects. The main structure of the SSD

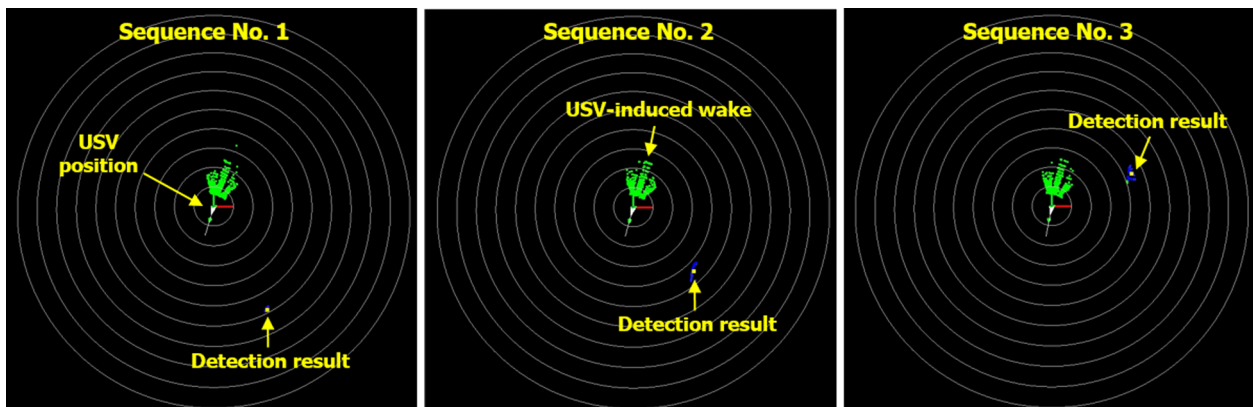


**FIGURE 7** Example of lidar-based target detection. Raw point cloud data are represented by green dots. The processed point cloud data after applying the point-distance-based-segmentation and weighting approach are represented by blue dots. The weighted center of the clusters is described by yellow dots [Color figure can be viewed at [wileyonlinelibrary.com](http://wileyonlinelibrary.com)]

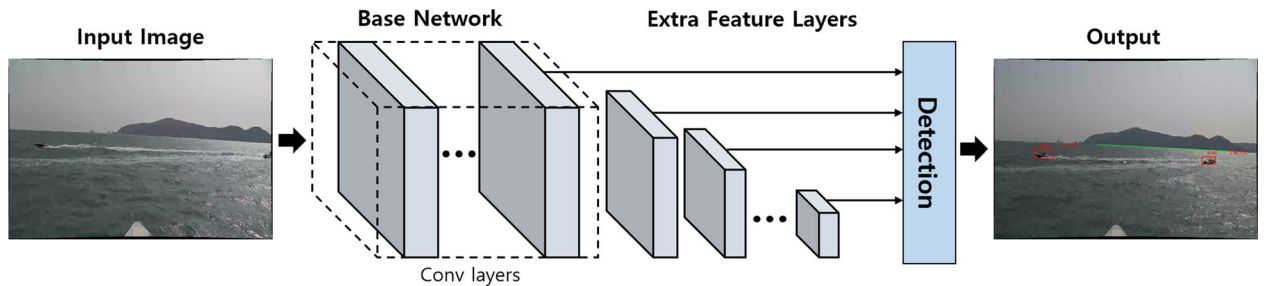


**FIGURE 8** Single-shot multibox detector architecture for automatic target detection based on deep learning [Color figure can be viewed at wileyonlinelibrary.com]

consists of a base network and an extra feature layer as shown in Figure 8. The base network is configured with a visual geometry group 16-layer model (VGG-16; Simonyan & Zisserman, 2014) network which is known to provide satisfactory classification results. The base network is located at the front layers and the extra feature layers are located at the back layers. The feature layers are used to detect the location of objects in the image coordinates and they are designed to become smaller as the layer becomes deeper to enhance the detection of objects with various sizes. At the end of the network, a loss value is computed by collecting the classification score and detection scores for each of the extra feature layers.

An appropriate data set and input image size are important components to train a neural network. We employ an SSD512 method in which the network is trained with  $512 \times 512$  input images and use data sets obtained from several maritime environments. We collect ship images from PASCAL VOC (Everingham, Van Gool, Williams, Winn, & Zisserman, 2010), Singapore Maritime Data set

(Prasad et al., 2017), and our field experiments using the USV system. The training images are selected to include various environmental and weather conditions, which enables robust ship detection of the network. The example detection results are described with bounding boxes as shown in Figures 9 and 10. The obtained target position in the image coordinates is converted to the relative measurements in the global coordinates as described in our previous works (Cho, Park, Kang, & Kim, 2015; Park, Kim, et al., 2015).

#### 4.2 | Tracking via sensor fusion

It is known that the optimal approach of multi-sensor tracking is to combine all observations from multiple detection sensors into a fusion-based tracking filter (Blackman & Popoli, 1999). However, this approach is not always preferred or allowed in practice, partially due to difficulty in data association with heterogeneous sensors and the

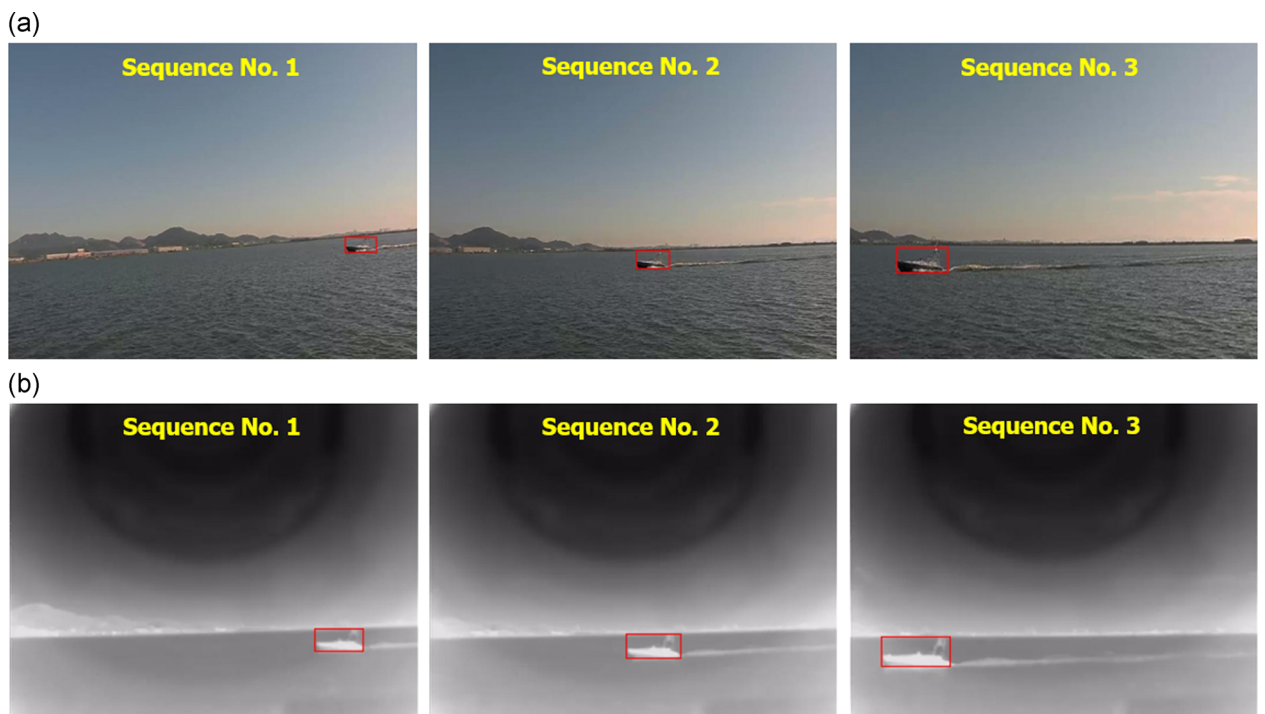


**FIGURE 9** Examples of ship detection results by the deep-learning approach. (a) Electro-optical camera-based detection results. (b) Infrared camera-based detection results [Color figure can be viewed at wileyonlinelibrary.com]

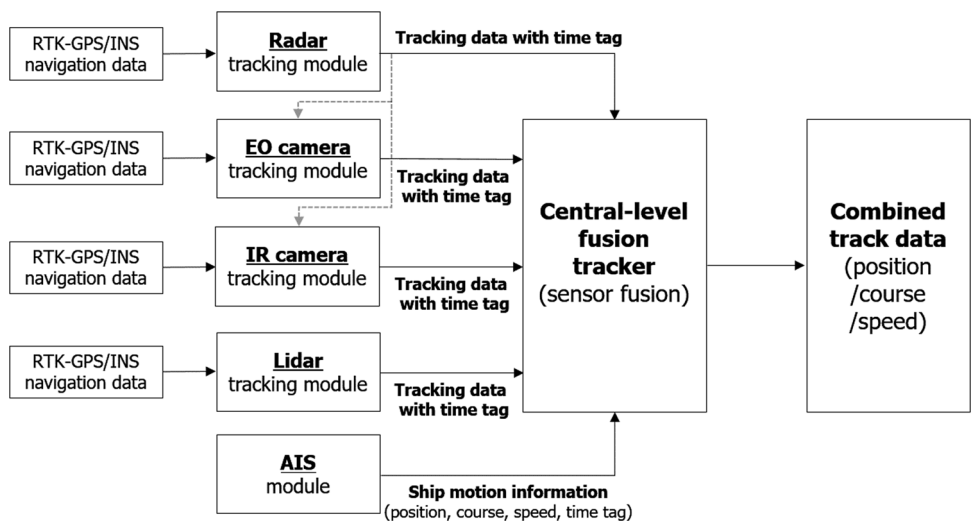


**FIGURE 10** Overall flowchart of the target tracking filter by sensor fusion. AIS, automatic identification system; EO, electro-optical; INS, inertial navigation system; IR, infrared; RTK-GPS, real-time kinematic global positioning system

relatively large computational load that cannot be easily distributed. In this study, each sensor maintains a local tracking filter (i.e., sensor-level tracking) using individual sensor measurements, and then the state estimation results by the sensor-level tracking filters are sent to a central-level fusion tracker to form a global track file by sensor fusion.

#### 4.2.1 | Sensor-level tracking

Given the detection results from sensor measurements, a target tracking filter based on an extended Kalman filter (EKF) is applied with a constant velocity model to estimate target motion (Bar-Shalom, Li, & Kirubarajan, 2004). A dual filter structure consisting of a confirmed track and a reserved track is employed to reduce the state estimation of false measurements by improving the robustness of the target tracking algorithm. A detected target is initially registered into the reserved track to determine whether it corresponds to a real target or a clutter by employing the well-known M-of-N logic (Bar-Shalom, Willett, & Tian, 2011). Once the target satisfies the M-of-N rule, it is moved into the confirmed track and its motion is consistently estimated in the tracking filter until the position uncertainty level becomes a pre-defined value.

A three-degrees-of-freedom (3 DOF) kinematic model is employed to represent the motion of the observing vehicle (i.e., USV) and the detected targets in the filter structure. The state vector of the observer is expressed by

$$\mathbf{x}_o = [x_o \ y_o \ \psi_o \ V_o]^T, \quad (3)$$

where  $x_o$  and  $y_o$  are the observer's position whose coordinate is defined in the global frame,  $\psi_o$  is the observer's heading, and  $V_o$  is the

longitudinal speed. The equations of the vehicle's motion can be written as

$$\dot{\mathbf{x}}_o = [V_o \cos \psi_o \ V_o \sin \psi_o \ 0 \ 0]^T. \quad (4)$$

For estimating the motion of the observer and the targets simultaneously, the augmented state vector is defined by cascading the observer state vector  $\mathbf{x}_o$  and the target state vector  $\mathbf{x}_{T^s} = [\mathbf{x}_{T_1^s}^T \ \mathbf{x}_{T_2^s}^T \ \dots]^T$ , where  $\mathbf{x}_{T_i^s} = [x_{T_i^s} \ y_{T_i^s} \ \psi_{T_i^s} \ V_{T_i^s}]^T$  represents the state vector of the  $i$ th registered target. The equations of the  $i$ th target motion can be written as

$$\dot{\mathbf{x}}_{T_i^s} = [V_{T_i^s} \cos \psi_{T_i^s} \ V_{T_i^s} \sin \psi_{T_i^s} \ 0 \ 0]^T. \quad (5)$$

This formulation allows for tracking multiple targets. As the number of registered targets increases, the total dimension of the target state vector grows. The equation of the system dynamics with the augmented state vector is expressed by

$$\dot{\mathbf{x}} = [\dot{\mathbf{x}}_o^T \ \dot{\mathbf{x}}_{T_1^s}^T \ \dot{\mathbf{x}}_{T_2^s}^T \ \dots]^T + \mathbf{w}, \quad (6)$$

where  $\mathbf{w}$  is the zero-mean Gaussian process noise reflecting the uncertainty in the system.

To update the motions of the observer and targets, two sets of measurements are used. The motion of the observer is corrected by measurement data set  $\mathbf{z}_o$ , which can be expressed as

$$\mathbf{z}_o = [z_x \ z_y \ z_\psi \ z_V]^T = [x_o \ y_o \ \psi_o \ V_o]^T + \mathbf{v}_o, \quad (7)$$

where  $z_x$ ,  $z_y$ ,  $z_\psi$ , and  $z_V$  represent the position, heading, and speed measurements provided by onboard navigation sensors.  $\mathbf{v}_o$  is the measurement noise, which is modeled as a zero-mean Gaussian distribution. The motion of each target is corrected by measurement data set  $\mathbf{z}_{T_i^s}$ , which can be expressed as

$$\mathbf{z}_{T_i} = \begin{bmatrix} z_{\beta_i} \\ z_{\rho_i} \end{bmatrix} = \begin{bmatrix} \tan^{-1}\left(\frac{y_{T_i^s} - y_0}{x_{T_i^s} - x_0}\right) - \psi_0 \\ \sqrt{(x_{T_i^s} - x_0)^2 + (y_{T_i^s} - y_0)^2} \end{bmatrix} + \mathbf{v}_{T_i}, \quad (8)$$

where  $z_{\beta_i}$  and  $z_{\rho_i}$  represent the relative bearing and range measurements for the  $i$ th target obtained from the target detection algorithms. Different values of the measurement noise  $\mathbf{v}_{T_i}$  are applied considering the accuracy and resolution of the detection sensors.

For data association between the existing targets in the filter state and the newly detected target measurements, the global nearest neighbor (GNN) method is employed (Blackman & Popoli, 1999). To find measurement-to-track pairs, an ellipsoidal gate is introduced for thresholding. The validity of each pair is determined by evaluating

$$d^2 = \bar{\mathbf{z}}^T S^{-1} \bar{\mathbf{z}}, \quad (9)$$

where  $d^2$  and  $S$  denote the normalized statistical distance and the innovation covariance matrix of measurement, respectively.  $\bar{\mathbf{z}}$  denotes the innovation vector defined by the difference between the expected measurement and the actual measurement.

#### 4.2.2 | Central-level track fusion

From the sensor-level tracking filters, a data set of the estimated target motion (i.e., position, course, and speed) and their associated uncertainties are provided to a fusion-based tracker. Among various types of fusion methods for track fusion (Drummond, 1996), a central-level fusion method is employed in this study, in which combined track data are maintained in an additional tracker and are periodically updated when the target states estimated in the sensor-level tracking filter are updated by the sensor measurements.

For persistent target tracking by sensor fusion, an additional tracker is established and central-level tracks are estimated by combining the sensor-level tracking results as described in Section 4.2.1. The state vector of the central tracker is augmented by cascading the combined target state vector  $\mathbf{x}_{T^c} = [\mathbf{x}_{T_1^c}^T \ \mathbf{x}_{T_2^c}^T \ \dots]^T$ , where  $\mathbf{x}_{T_i^c} = [x_{T_i^c} \ y_{T_i^c} \ \psi_{T_i^c} \ V_{T_i^c}]^T$  describes the state vector of the  $i$ th registered target.

For the track association between the combined tracks and the sensor-level tracks, all of the estimated kinematic quantities including position, course, and speed are considered in the GNN method and the similarity between the tracks is evaluated. The equations associated with track fusion can be written as

$$\begin{aligned} \hat{\mathbf{x}}_{T^c} &= \hat{\mathbf{x}}_{T^s} + C[\hat{\mathbf{x}}_{T^c} - \hat{\mathbf{x}}_{T^s}], \\ C &= [P_{T^c} - P_{T^s}]U_{cs}^{-1}, \\ U_{cs} &= P_{T^c} + P_{T^s} - P_{T^{cs}} - P_{T^{sc}}, \end{aligned} \quad (10)$$

where  $\hat{\mathbf{x}}_{T^s}$  and  $\hat{\mathbf{x}}_{T^c}$  represent the track states from the sensor-level tracking and the fusion tracker, respectively.  $P_{T^s}$  and  $P_{T^c}$  are the associated covariances of the individual sensor track and the combined track, respectively.  $P_{T^{cs}}$  is the cross-covariance between

the combined track and the sensor-level track, which reflects the time correlation associated with the sensor-level track that is used to update the combined track. For practical applications, the elements of the cross-covariance are estimated by the approximation method as described in Bar-Shalom and Li (1995).

In addition to the sensor-level track data, the motion information from AIS is used to update the combined track data in the central-level fusion tracker. For this, a track state is organized using the obtained motion information including position, course and speed. However, AIS data may not be always available and reliable because of various factors such as data inaccuracies, missing measurements, packet dropouts, communication delays, and so forth. Considering these error properties, the uncertainties of AIS data are appropriately reflected in the error covariance matrix for fusing all the measurements for target tracking.

#### 4.2.3 | Time-delayed measurement (track) update

To update the track state estimate after the data association in the sensor-level tracking, there is a time delay between the point of measurement generation and the point of the motion update using the measurement in the tracking filter. If the sampling rate to provide new sensor measurements is relatively higher than that of the filter update rate, the error driven by the time delay is negligible (Han, Son, & Kim, 2019). However, the sensor-level tracking filter with a relatively low sampling rate (e.g., radars) requires an additional technique to achieve satisfactory tracking performance by compensating for the delay effects. For this, a target state which is estimated in the tracking filter is retrodicted to the time of measurement generation and the residual (i.e., innovation) is formed, which represents the difference between the retrodicted target state and the newly obtained sensor measurement. The residual term is used to update the target motion state in the filtering framework and the associated covariance matrix is updated as described in Bar-Shalom and Li (1995). The updated state and its covariance are then propagated to the current time. In the central-level fusion tracker, a similar approach is applied to compensate the time delay between the point of a track formation in the sensor-level tracking filter and the point of the motion update in the fusion tracker.

### 4.3 | Collision-avoidance control

#### 4.3.1 | Configuration of the collision avoidance system

The A\* algorithm has been commonly used for computing a route for ship collision avoidance (Rhee & Lee, 1996). In this study, we apply the collision avoidance algorithm in which changeable action space is employed to consider the change of the level of collision risk (N. Son, Furukawa, Kim, & Kijima, 2009; N.-s. Son & Kim, 2018).

### 4.3.2 | Collision-avoidance algorithm

This collision avoidance procedure consists of three steps (N.-s. Son & Kim, 2018). In the first step, the action space is generated using the motion information of both the USV and the target ships at the current state ( $t = t_0$ ). In the second step, the generated action space is re-built by considering the collision risk at the future state ( $t = t_0 + \Delta t$ ), which is calculated by a fuzzy inference algorithm based on the time to the closest point of approach (TCPA) and distance to the closest point of approach (DCPA; N. Son et al., 2009).

Figure 11 shows a graphical representation of the construction of the action space. The layer is constructed perpendicular to a line between the previous and next waypoints. The spacing between the layers is set to be proportional to the length of the ship, and the proportional coefficient is adaptively changed depending on the collision risks. The number of branches from the node can be also changed adaptively according to the collision risk. In the last step, the optimal route is selected among the branching paths considering both the cost function associated with the collision risk and the COLREGs (Commandant, 1999; N. Son et al., 2009).

## 5 | FIELD EXPERIMENT

To verify the practical feasibility of the developed autonomous navigation algorithms, an extensive set of field experiments were performed under various marine traffic scenarios using the Aragon USV system. Various types of small-size vessels (Figure 12a) were considered as traffic vessels. They are common obstacles in a maritime traffic situation and their position information is not always available from AIS data messages. To monitor the status and change the operating parameters remotely, a mobile ground control station was set up on two vehicles shown in Figure 12b. A self-rotating

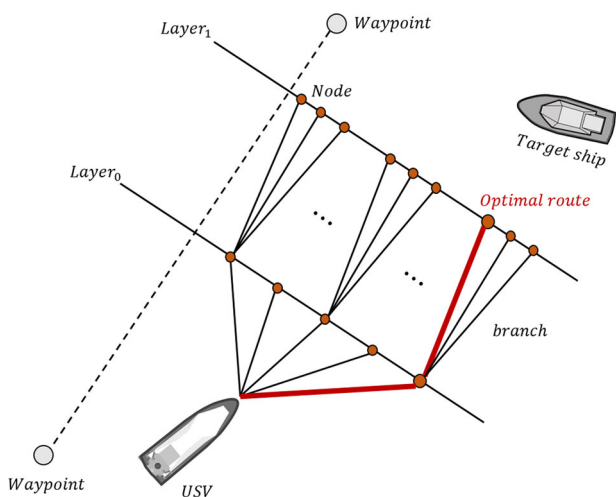


**FIGURE 11** Graphical representation of the changeable action space search method based on A\*. The thick solid line describes the optimal route determined based on the cost function [Color figure can be viewed at [wileyonlinelibrary.com](http://wileyonlinelibrary.com)]

communications antenna was mounted on one of the vehicles for wireless communication between the control center and the USV.

A customized graphical user interface was developed to change the parameters associated with the autonomy algorithms (e.g., guidance mode, control gains, filter parameters, and navigation mode flags) and to command an autonomous navigation mode by an operator. The autonomous navigation algorithms were implemented in C++ using SPx software for radar image processing (Cambridge Pixel Ltd, 2018) and point cloud library (PCL) for lidar data processing (Rusu & Cousins, 2011).

In this paper, we summarize the results from two field experiments among several field tests performed during the development of the USV system. Figure 13 represents the scenarios of these two field tests; the first one conducted in Asan-ho near the Western Korean sea (left) and the second one conducted in Suyoung Bay located in the southern Korean sea (right). Three power boats of approximately 8 m length were used as target vessels in port-crossing, starboard-crossing, and head-on approaching situations. The target vessels were set to approach the USV consecutively to generate challenging encounter situations. The speeds of the USV and the moving targets were set to be 10 knots. The target vessels were manually operated by human operators and AIS devices were mounted on the vessels to obtain the ground-truth data of their motion.

Figure 14 shows the results of the first field experiment. To estimate trajectories of the target vessels, the pulse radar, the lidar, and the EO/IR cameras were used, and the resulting trajectories are presented in Figure 14a. The solid lines describe the estimated target trajectory in the central-level fusion tracker where all the sensor-level tracking data are combined; the dotted line describes the USV trajectory by the onboard motion sensor. The AIS data for the three target vessels were collected to evaluate the target tracking performance, and these are denoted as black squares. The estimated trajectories using the onboard detection sensors satisfactorily follow the ground-truth trajectories. Furthermore, the relative ranges of the target vessels with respect to the USV are presented in Figure 14b. The solid line represents the estimated relative range obtained by the sensor fusion and the black squares represent the relative range obtained by the AIS. The tracking data, which are obtained from the sensor-level tracking filters and combined in the central-level fusion tracker, are represented by blue circles (radar), magenta plus signs (EO), cyan crosses (lidar), and yellow asterisks (IR). The targets could be detected until the relative range approached approximately 100–130 m using the pulse radar, and then, in the radar blind zone, they were persistently detected by the camera and lidar sensors. The estimated course and speed of the approaching targets are also presented in Figure 14c. The solid line with circles represents the course (left) and speed (right) information estimated in the central-level fusion tracker. The estimated motion information closely follows the ground-truth data (solid line with black squares), which shows satisfactory state estimation performance of the multi-sensor tracking algorithm.

Figure 15 shows the results of the second field experiment. Here, the motion information of surrounding vessels, including traffic ships



**FIGURE 12** Field test configuration. (a) Target vessels used for the field tests. (b) Mobile ground control station set up on two vehicles [Color figure can be viewed at [wileyonlinelibrary.com](http://wileyonlinelibrary.com)]

and buoys, could be obtained by the AIS receiver mounted on the USV platform; hence the AIS data were also combined in the central-level fusion tracker. In the left figures, the target vessels' trajectories estimated in the extended central-level fusion tracker are described by red squares, and their course and speed are described by the direction and length of black lines at the current position. The estimated motion data of the target vessels were transmitted into the framework of the

collision avoidance system, and the nodes generated by the collision avoidance algorithm are described by black dots. In accordance with the COLREGs, the USV has an obligation to keep its course and speed with respect to the ship approaching from the port side (target #1). However, the USV altered its course to the starboard side to escape the risky situation because the give-way vessel did not take any rule-compliant maneuver. In the encounter with the starboard-crossing vessel (target

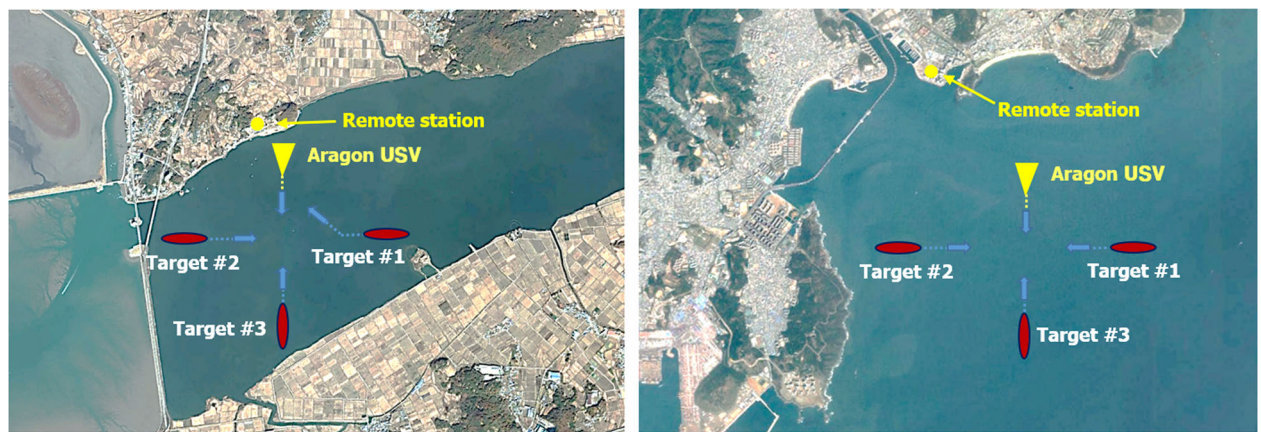


**FIGURE 13** Experimental scenarios for multiple target tracking and collision avoidance in Asan-ho (left) and in Suyoung Bay (right). Three target vessels were set to approach consecutively the unmanned surface vehicle (USV) during the field tests [Color figure can be viewed at [wileyonlinelibrary.com](http://wileyonlinelibrary.com)]

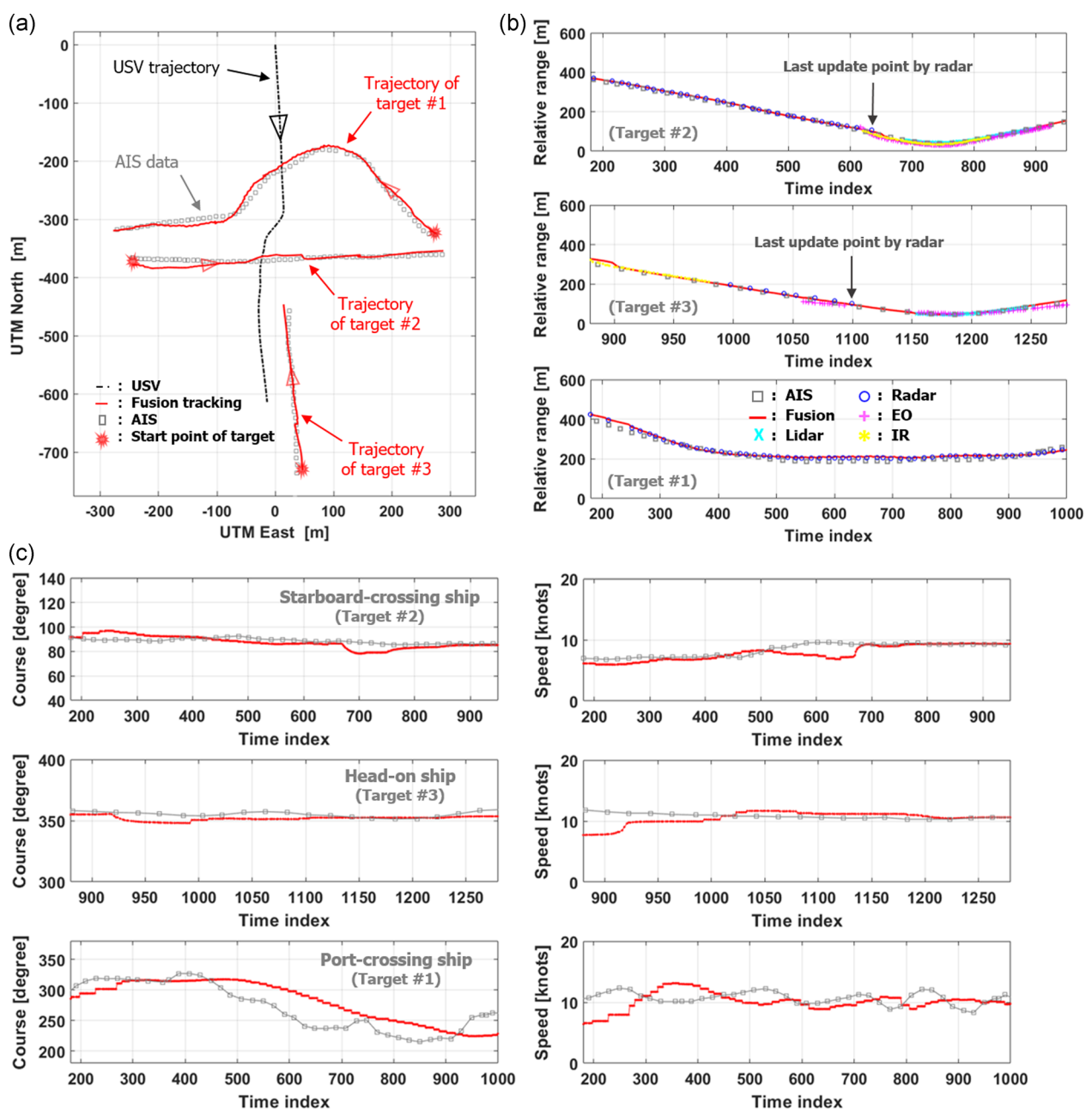


**FIGURE 14** Experimental results of the multiple target tracking by sensor fusion. (a) Estimated trajectories of the target vessels. (b) Relative range of the target ships with respect to the unmanned surface vehicle. (c) Estimated course (left) and speed (right) of the target ships. AIS, automatic identification system; EO, electro-optical; IR, infrared [Color figure can be viewed at [wileyonlinelibrary.com](http://wileyonlinelibrary.com)]

#2) and the head-on vessel (target #3), the USV is the give-way vessel, so our own ship altered its course to starboard side for collision avoidance as shown in Figure 15. The snapshots of the collision avoidance situations are shown in the figure.

## 6 | CONCLUSIONS

This study presented a newly developed USV system with an autonomous navigation capability and its field test results. The developed system includes the vehicle hardware platform, the

operational software algorithms, and the integration of hardware and software components for unmanned vehicle autonomy. In the development process, we focused on the target tracking technique by sensor fusion to achieve persistent and reliable autonomous situational awareness capability and the automatic collision avoidance system for safe vehicle operation. The performance and practical feasibility of the developed vehicle and autonomous navigation algorithms were successfully demonstrated through field experiments in real-sea environments.

It is worthwhile to note some operational difficulties we experienced and the lessons learned from the field experiments. The key limiting factor of autonomous navigation is the performance in

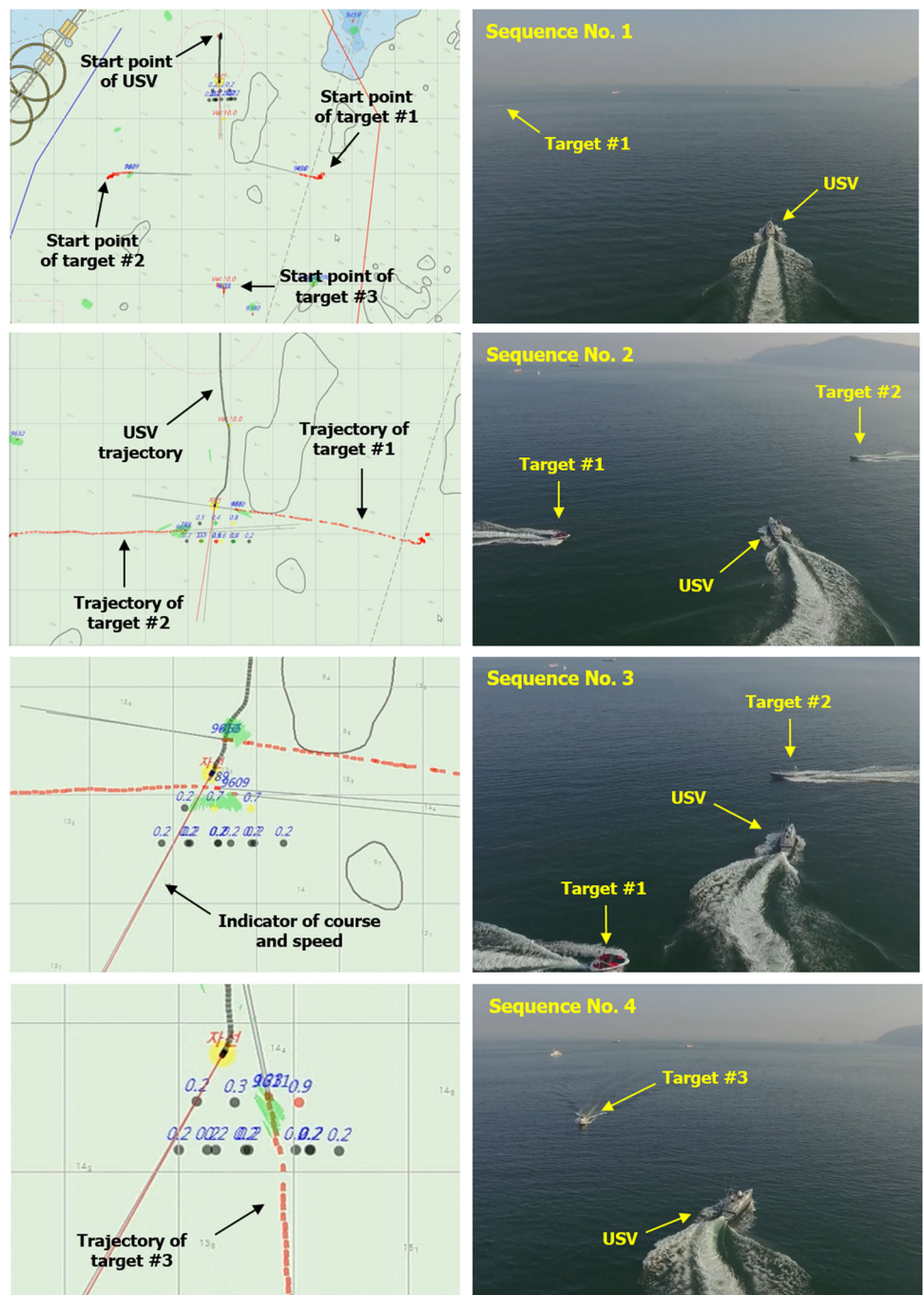


**FIGURE 15** Experimental results of the automatic collision avoidance. On the left side figures, the trajectory of the USV and target ships are overlaid on an electronic navigation chart. The course and speed of target ships are represented by the direction and length of black lines at their current positions. The right figures show the corresponding snapshots captured by a drone when the USV encountered the moving target ships [Color figure can be viewed at [wileyonlinelibrary.com](http://wileyonlinelibrary.com)]

situational awareness provided by onboard perception devices such as radar, lidar and camera sensors. Among them, the pulse radar is a sensor with the longest detection range. However, the rotational frequency of the antenna rotation is approximately 0.5 Hz, and this limits the update rate of radar images. Moreover, each ray measurement in one image is generated at a different time. As a result, every target had to be updated asynchronously depending on the relative bearing of targets in the sensor-fixed frame. Otherwise, the tracking

performance degraded significantly. Also, the lidar and camera were used to detect objects on the water surface at relatively close range covering the radar's blind zone. However, particularly in windy and rough sea conditions, a lot of noise and unwanted measurements were included, and they need to be eliminated before applying the feature extraction algorithm. The noise and clutter in the lidar data could be efficiently reduced by employing the height-based thresholding scheme described in Section 4.1.2. However, the same thresholding

scheme cannot be used to remove the noise in the camera image, because no 3D structure is provided in the camera image. For noise removal, after some trials with conventional computation-vision techniques which were not quite successful, deep-learning techniques were employed. Even with a moderate amount of labeled data, more satisfactory and reliable performance could be achieved by deep learning.

From our experiments conducted during the development of the USV system, we found that the active sensors such as radar and lidar provide more reliable detection performance in marine environments than the passive sensors such as cameras. To achieve reliable and satisfactory performance, various parameters of hardware system settings and autonomous navigation algorithms were tuned depending on experimental conditions for detecting the small-sized target vessels. Among them, the parameter tuning of the camera-based tracking algorithm was sensitive and required significant time to fit the experimental condition. In our sensor suite, the blind zone of the pulse radar was approximately 80–200 m depending on environmental conditions. The cameras could cover mid-range obstacles below approximately 350 m and the lidar could cover short-range obstacles below approximately 80 m to detect the target vessels. Thus, the camera-based tracking technique was necessary for persistent target tracking by updating the motion of targets in the radar's blind zone over the detectable range of the lidar. Recently, more precise and higher-resolution lidar with long-range detection capability has been developed for self-driving car applications. Using a long-range lidar and a radar to detect surrounding obstacles for persistent target motion analysis and using a camera to identify the type of the detected obstacles (e.g., buoy, sails, or barges) may be a preferred perception strategy to improve maritime autonomy.

## ACKNOWLEDGMENTS

This study was supported by the project titled "Development of multi-purpose autonomous unmanned surface vehicle (PMS3870)" under the financial support of Korea Ministry of Oceans and Fisheries, Korea. Also, this study was a part of the project entitled "Development of situation awareness and autonomous navigation technology of unmanned surface vehicle based on the artificial intelligence (PES3050)" funded by the Korea Research Institute of Ships and Ocean Engineering.

## ORCID

Jinwhan Kim  <http://orcid.org/0000-0001-6886-2449>

## REFERENCES

- Bar-Shalom, Y., & Li, X.-R. (1995). *Multitarget-multisensor tracking: Principles and techniques*. Storrs, CT: YBs.
- Bar-Shalom, Y., Li, X. R., & Kirubarajan, T. (2004). *Estimation with applications to tracking and navigation: Theory algorithms and software*. New York: John Wiley & Sons.
- Bar-Shalom, Y., Willett, P. K., & Tian, X. (2011). *Tracking and data fusion*. Storrs, CT: YBS Publishing.
- Benjamin, M. R., Leonard, J. J., Curcio, J. A., & Newman, P. M. (2006). A method for protocol-based collision avoidance between autonomous marine surface craft. *Journal of Field Robotics*, 23(5), 333–346.
- Bertram, V. (2008). Unmanned surface vehicles-a survey. *Skibsteknik Selskab, Copenhagen, Denmark*, 1, 1–14.
- Blackman, S., & Popoli, R. (1999). *Design and analysis of modern tracking systems(book)*. Norwood, MA: Artech House.
- Blaich, M., Rosenfelder, M., Schuster, M., Bittel, O., & Reuter, J. (2012). Fast grid based collision avoidance for vessels using A\* search algorithm. In *proceedings of the International Conference on Methods and Models in Automation and Robotics*, Miedzyzdroje, Poland (pp. 385–390).
- Bloisi, D., & Iocchi, L. (2009). Argos-a video surveillance system for boat traffic monitoring in venice. *International Journal of Pattern Recognition and Artificial Intelligence*, 23(07), 1477–1502.
- Borges, G. A., & Aldon, M.-J. (2004). Line extraction in 2D range images for mobile robotics. *Journal of intelligent and Robotic Systems*, 40(3), 267–297.
- Cambridge Pixel Ltd. (2018). [online]. Retrieved from <http://www.cambridgepixel.com>
- Cho, Y., Park, J., Kang, M., & Kim, J. (2015). Autonomous detection and tracking of a surface ship using onboard monocular vision. In *Proceedings of the International Conference on Ubiquitous Robots and Ambient Intelligence*, Goyang, Korea (pp. 26–31).
- Commandant, U. C. G. (1999). International regulations for prevention of collisions at sea, 1972 (72 COLREGS). US Department of Transportation, US Coast Guard, COMMANDANT INSTRUCTION M, 16672. 2D.
- Curcio, J., Leonard, J., & Patrikalakis, A. (2005). Scout-a low cost autonomous surface platform for research in cooperative autonomy. In *Proceedings of MTS/IEEE OCEANS*, Washington, DC (pp. 725–729).
- Drummond, O. E. (1996). Track fusion with feedback. In *Proceedings of the SPIE 2759, Signal and Data Processing of Small Targets*, Orlando, Florida, United States (pp. 342–361).
- Elfes, A. (1989). Using occupancy grids for mobile robot perception and navigation. *Computer*, 22(6), 46–57.
- Elkins, L., Sellers, D., & Monach, W. R. (2010). The autonomous maritime navigation (AMN) project: Field tests, autonomous and cooperative behaviors, data fusion, sensors, and vehicles. *Journal of Field Robotics*, 27(6), 790–818.
- Eum, H., Bae, J., Yoon, C., & Kim, E. (2015). Ship detection using edge-based segmentation and histogram of oriented gradient with ship size ratio. *International Journal of Fuzzy Logic and Intelligent Systems*, 15(4), 251–259.
- Everingham, M., Van Gool, L., Williams, C. K., Winn, J., & Zisserman, A. (2010). The pascal visual object classes (VOC) challenge. *International Journal of Computer Vision*, 88(2), 303–338.
- Farina, A. (1999). Target tracking with bearings-only measurements. *Signal Processing*, 78(1), 61–78.
- Frew, E. W., & Rock, S. M. (2003). Trajectory generation for constant velocity target motion estimation using monocular vision. In *Proceedings of the IEEE International Conference on Robotics and Automation*, Taipei, Taiwan, (Vol. 3, pp. 3479–3484).
- Hagen, I. B., Kufoalor, D., Brekke, E., & Johansen, T. (2018). Mpc-based collision avoidance strategy for existing marine vessel guidance systems. In *Proceedings of the International Conference on Robotics and Automation*, Brisbane, Australia (pp. 7618–7623).
- Hamerly, G., & Elkan, C. (2003). Learning the k in k-means. In *Neural Information Processing Systems* (pp. 2003). Cambridge, MA: MIT Press.
- Han, J., & Kim, J. (2019). Three-dimensional reconstruction of a marine floating structure with an unmanned surface vessel. *IEEE Journal of Oceanic Engineering*, 44(4), 984–996.
- Han, J., Kim, J., & Son, N.-s. (2017). Persistent automatic tracking of multiple surface vessels by fusing radar and lidar. In *Proceedings of the MTS/IEEE OCEANS*, Aberdeen, UK (pp. 1–5).

- Han, J., Park, J., Kim, T., & Kim, J. (2015). Precision navigation and mapping under bridges with an unmanned surface vehicle. *Autonomous Robots*, 38(4), 349–362.
- Han, J., Son, N.-s., & Kim, J. (2019). Automatic target tracking with time-delayed measurements for unmanned surface vehicles. In *Proceedings of the SPIE 11197, SPIE Future Sensing Technologies*, Tokyo, Japan (pp. 184–189).
- Hu, W.-C., Yang, C.-Y., & Huang, D.-Y. (2011). Robust real-time ship detection and tracking for visual surveillance of cage aquaculture. *Journal of Visual Communication and Image Representation*, 22(6), 543–556.
- Huntsberger, T., Aghazarian, H., Howard, A., & Trotz, D. C. (2011). Stereo vision-based navigation for autonomous surface vessels. *Journal of Field Robotics*, 28(1), 3–18.
- Kazimierski, W. (2011). Determining of marine radar target movement models for the needs of multiple model neural tracking filter. In *Proceedings of the International Radar Symposium*, Leipzig, Germany (pp. 611–616).
- Kuwata, Y., Wolf, M. T., Zarzhitsky, D., & Huntsberger, T. L. (2014). Safe maritime autonomous navigation with COLREGS, using velocity obstacles. *IEEE Journal of Oceanic Engineering*, 39(1), 110–119.
- Liggins, M., II, Hall, D., & Llinas, J. (2017). *Handbook of multisensor data fusion: Theory and practice*. Boca Raton: CRC Press.
- Liu, W., Anguelov, D., Erhan, D., Szegedy, C., Reed, S., Fu, C.-Y., & Berg, A. C. (2016). SSD: Single shot multibox detector. In *proceedings of the European Conference on Computer Vision*, Amsterdam, Netherlands (pp. 21–37). Springer.
- Ma, F., Chen, Y.-w., Yan, X.-p., Chu, X.-m., & Wang, J. (2016). A novel marine radar targets extraction approach based on sequential images and bayesian network. *Ocean Engineering*, 120, 64–77.
- Nikolić, D., Popović, Z., Borenović, M., Stojković, N., Orlić, V., Dzvonkovskaya, A., & Todorović, B. M. (2016). Multi-radar multi-target tracking algorithm for maritime surveillance at OTH distances. In *Proceedings of the International Radar Symposium*, Krakow, Poland (pp. 1–6).
- Papadopoulos, G., Kurniawati, H., Shariff, A. S. B. M., Wong, L. J., & Patrikalakis, N. M. (2014). Experiments on surface reconstruction for partially submerged marine structures. *Journal of Field Robotics*, 31(2), 225–244.
- Park, J., Cho, Y., Yoo, B., & Kim, J. (2015). Autonomous collision avoidance for unmanned surface ships using onboard monocular vision. In *Proceedings of the MTS/IEEE OCEANS*, Washington, USA (pp. 1–6).
- Park, J., Kim, J., & Son, N.-S. (2015). Passive target tracking of marine traffic ships using onboard monocular camera for unmanned surface vessel. *Electronics Letters*, 51(13), 987–989.
- Perera, L. P., Ferrari, V., Santos, F. P., Hinostroza, M. A., & Soares, C. G. (2015). Experimental evaluations on ship autonomous navigation and collision avoidance by intelligent guidance. *IEEE Journal of Oceanic Engineering*, 40(2), 374–387.
- Prasad, D. K., Rajan, D., Rachmawati, L., Rajabally, E., & Quek, C. (2017). Video processing from electro-optical sensors for object detection and tracking in a maritime environment: A survey. *IEEE Transactions on Intelligent Transportation Systems*, 18(8), 1993–2016.
- Premebida, C., & Nunes, U. (2005). Segmentation and geometric primitives extraction from 2D laser range data for mobile robot applications. *Robotica*, 17–25.
- Redmon, J., & Farhadi, A. (2017). Yolo9000: better, faster, stronger. *The IEEE Conference on Computer Vision and Pattern Recognition (CVPR)* (pp. 7263–7271).
- Ren, S., He, K., Girshick, R., & Sun, J. (2017). Faster r-cnn: Towards real-time object detection with region proposal networks. *IEEE Transactions on Pattern Analysis & Machine Intelligence*, 39(6), 1137–1149.
- Rhee, K., & Lee, H. (1996). Development of a collision avoidance system considering the navigation plan. In *Proceedings of the International Conference MARSIM*, Copenhagen, Denmark (pp. 341–348).
- Rohling, H. (1983). Radar CFAR thresholding in clutter and multiple target situations. *IEEE Transactions on Aerospace and Electronic Systems*, 19(4), 608–621.
- Rusu, R. B., & Cousins, S. (2011). 3D is here: Point Cloud Library (PCL). In *Proceedings of the IEEE International Conference on Robotics and Automation*, Shanghai, China (pp. 1–4).
- Simonyan, K., & Zisserman, A. (2014). Very deep convolutional networks for large-scale image recognition. *arXiv preprint arXiv: 1409.1556*.
- Son, N., Furukawa, Y., Kim, S., & Kijima, K. (2009). Study on the collision avoidance algorithm against multiple traffic ships using changeable action space searching method. *Journal of the Korean Society for Marine Environment & Energy*, 12(1), 15–22.
- Son, N.-s., & Kim, S.-Y. (2018). On the sea trial test for the validation of an autonomous collision avoidance system of unmanned surface vehicle, aragon. In *Proceedings of the MTS/IEEE OCEANS*, Charleston, SC, USA (pp. 1–5).
- Sonnenburg, C., Gadre, A., Horner, D., Kragelund, S., Marcus, A., Stilwell, D. J., & Woolsey, C. (2010). Control-oriented planar motion modeling of unmanned surface vehicles. In *Proceedings of the MTS/IEEE OCEANS*, Seattle, WA, USA (pp. 1–10).
- Sonnenburg, C. R., & Woolsey, C. A. (2013). Modeling, identification, and control of an unmanned surface vehicle. *Journal of Field Robotics*, 30(3), 371–398.
- Tang, P., Zhang, R., Liu, D., Huang, L., Liu, G., & Deng, T. (2015). Local reactive obstacle avoidance approach for high-speed unmanned surface vehicle. *Ocean Engineering*, 106, 128–140.
- Vivone, G., Braca, P., & Errasti-Alcalá, B. (2015). Extended target tracking applied to x-band marine radar data. In *Proceedings of the MTS/IEEE OCEANS*, Genova, Italy (pp. 1–6).
- Wolf, M. T., Assad, C., Kuwata, Y., Howard, A., Aghazarian, H., Zhu, D., Lu, T., Trebi-Ollennu, A., & Huntsberger, T. (2010). 360-degree visual detection and target tracking on an autonomous surface vehicle. *Journal of Field Robotics*, 27(6), 819–833.
- Zhang, X., Wang, H., & Cheng, W. (2017). Vessel detection and classification fusing radar and vision data. In *Proceedings of the International Conference on Information Science and Technology*, Da Nang, Vietnam (pp. 474–479).
- Zhang, Y., Li, Q.-Z., & Zang, F.-N. (2017). Ship detection for visual maritime surveillance from non-stationary platforms. *Ocean Engineering*, 141, 53–63.

**How to cite this article:** Han J, Cho Y, Kim J, Kim J, Son N-S, Kim SY. Autonomous collision detection and avoidance for ARAGON USV: Development and field tests. *J Field Robotics*. 2020;37:987–1002. <https://doi.org/10.1002/rob.21935>